RSC Advances

PAPER

View Article Online
View Journal | View Issue

Check for updates

Cite this: *RSC Adv.*, 2018, **8**, 31066

Triangular radial Nb_2O_5 nanorod growth on *c*-plane sapphire for ultraviolet-radiation detection†

Kwan-Woo Kim,‡[a] Bum Jun Kim,‡[b] Sang Hoon Lee,[a] Tuqeer Nasir,[b] Hyung-Kyu Lim,[a] Ik Jun Choi,[a] Byung Joo Jeong,[a] Jaeyeong Lee,[c] Hak Ki Yu[c] and Jae-Young Choi*[ab]

Received 20th July 2018
Accepted 27th August 2018

DOI: 10.1039/c8ra06139d

rsc.li/rsc-advances

Nb_2O_5 nanostructures with excellent crystallinities were grown on *c*-plane sapphire and employed for ultraviolet-(UV)-radiation detection. The triangular radial Nb_2O_5 grown on the *c*-sapphire substrate had a 6-fold symmetry with domain matching epitaxy on the substrate. Owing to the radial growth, the nanorods naturally connected when the deposition time increased. This structure can be used as a UV-detector directly by depositing macroscale electrodes without separation of a single nanorod and e-beam lithography process. It was confirmed that electric reactions occur at different UV irradiation wavelengths (254 nm and 365 nm).

Introduction

Ultraviolet rays (UV) are electromagnetic waves with shorter wavelengths than those of visible light, mainly in the range of 200 nm to 400 nm.[1] UV irradiation affecting our lives can be divided into two types: (i) generated from the sun, reaching the earth through cosmic radiation, and (ii) those emerging from various chemical reactions on the earth. UV irradiation generated from the sun is mostly absorbed by various molecules in the atmosphere (CO_2, H_2O, *etc.*); radiation reaching the surface is in the region of UV-A (320–400 nm).[1] UV-A can have positive effects, such as sterilisation, or side effects such as occurrence of skin cancer. On the other hand, UV radiation generated by various chemical reactions produced by humans varies from UV-A to UV-C (UV-B: 290–320 nm and UV-C: 200–290 nm). Both efficient use of the generated UV radiation and its blockage for safety purposes are important.

In this regard, one of the most important factors is the efficient UV detection. Theoretically, one of the best approaches to detect UV irradiation is to measure changes in electrical conductivity of an UV-irradiated material with band gap.[1–5] It is important to select a material with an appropriate band gap (E_g > 3.1 eV) in order to detect UV radiation in the range of 200 nm to 400 nm (UV-A to UV-C regions). However, if the band gap is too large, the material is close to insulator and the electron excitation effect due to UV absorption is not sufficient to detect.

In this study, we aimed to implement a UV-radiation detector using Nb_2O_5 with an ideal band-gap energy in the range of 3.5 eV to 4.8 eV (photon energy of 354 nm to 258 nm)[6–8] and chemical stability[9–11] for UV detection. It has already been shown by Fang *et al.*[12] and Liu *et al.*[13] that Nb_2O_5 can be used as a UV detector and has high responsivity. In addition, the Nb_2O_5 UV detector was recently synthesized using a simple and low cost hydrothermal method.[14] In order to develop the UV-detector using Nb_2O_5, materials with good crystallinities should be synthesised, as when a defect is present in Nb_2O_5, light absorption occurs due to the defect levels (532 nm: 2.3 eV and 808 nm: 1.5 eV). In the case of thin-film or bulk syntheses, the possibility of occurrence of defects such as grain boundaries in the synthesised material increases. We aimed to synthesise nanoscale single-crystal Nb_2O_5 (various structures of Nb_2O_5 nanomaterials were used for applications to gas sensors,[15,16] photo-catalysts,[17,18] photo-detectors,[12,19] batteries,[20,21] solar cells,[22,23] *etc.*). In addition, if the detector device is fabricated using a single nanorod,[11,24–28] the fabrication is complex (such as e-beam lithography), leading to a lower productivity and higher process costs. Therefore, in this study, synthesis conditions (substrate type and orientation, precursor of Nb, growth temperature, and reaction/carrier gas) were investigated so that synthesised Nb_2O_5 nanostructures could be naturally connected to each other to enable to immediately use the device when only macroscale electrodes are deposited.

Experimental

Growth of Nb_2O_5 nanostructures

The growth of Nb_2O_5 was performed on a single-crystal *c*-plane sapphire substrate (Namkang Hi-tech Co., Ltd., SaR 100-500)

---

[a] School of Advanced Materials Science and Engineering, Sungkyunkwan University, Suwon, 16419, Korea. E-mail: jy.choi@skku.edu

[b] SKKU Advanced Institute of Nanotechnology (SAINT), Sungkyunkwan University, Suwon, 16419, Korea

[c] Department of Materials Science and Engineering, Department of Energy Systems Research, Ajou University, Suwon, 16499, Korea

† Electronic supplementary information (ESI) available. See DOI: 10.1039/c8ra06139d

‡ These authors contributed equally to this study.

using a quartz tube furnace. $NbCl_5$ (Alfa Aesar, #11548), used as a Nb precursor, was placed in a stainless-steel canister, which was heated by a heating mantle. The sublimed $NbCl_5$ and Ar carrier gas were introduced into the tube through a 1/4 inch stainless-steel gas line, which was wrapped and heated by a commercial heating tape. The temperatures of the canister and line were maintained at 140 °C and 160 °C, respectively.

For cleaning, the sapphire substrates were sonicated in acetone, alcohol, and deionised (DI) water for 15 min in each solvent. The sapphire substrates were then loaded into the tube furnace and the system was pumped down to vacuum and refilled with Ar gas to obtain atmospheric pressure. The furnace temperature was increased to 900 °C within 40 min in Ar environment with an Ar gas flow of 200 sccm. After the temperature reached 900 °C, the growth of Nb_2O_5 was initiated by introducing another flow (200 sccm) of Ar carrier gas through the canister to the furnace. After the growth, the Nb-precursor supply line was closed, and the samples were rapidly cooled down under the Ar environment.

Analysis and measurement

An X-ray diffractometer (Bruker D8-Advance with monochromated Cu-$K_{\alpha 1}$ radiation; scan rate of $0.05° \, s^{-1}$) was used for identification of the sample. A pole figure analysis was performed to study the symmetry of the sample using an X-ray diffractometer (PANalytical, X'pert PRO using Cu-K_α radiation, χ: 0–75° and φ: 0–360° at 2θ of 25°). The surface morphology and cross-section structure of the sample were investigated by SEM (Hitachi, S-4800). Transmission electron microscopy (TEM) (JEOL, JEM-2100F, at 200 kV) was employed to analyse the structures and growth directions of the rods. A UV/visible spectrometer (Shimadzu, UV-3600) was used to measure the optical transmittance of the material. A current–voltage (I–V) curve and time-dependent response of the UV detector were obtained using a probe station (MSTECH, MST5000). A single-wavelength (254 nm/365 nm) UV lamp (VILBER, VL-215 LC) was used as the UV source.

Results and discussion

To understand the effect of the substrate on the growth of the Nb_2O_5 nanorods, we performed SEM on Nb_2O_5 synthesised on three types of substrates (SiO_2/Si, graphene-coated Ni foil, and c-plane (0006) sapphire substrate; see Fig. 1a). On the graphene/Ni surface, irregularly sized structures are observed, while on the other two substrates (SiO_2/Si and c-plane sapphire), nanorods with uniform sizes were synthesised. The irregularities observed on the graphene surface can be interpreted as a phenomenon in which niobium oxide nuclei cannot be easily generated owing to the low surface energy of the graphene surface (40–50 mJ m^{-2}) compared to those of SiO_2/Si (~800 mJ m^{-2}) and c-plane sapphire (~1900 mJ m^{-2}).[29–31] X-ray diffraction (XRD) was performed to characterise the nanorod alignments on SiO_2/Si and c-plane sapphire (Fib. 1b). The Nb_2O_5 nanorods deposited on the c-plane sapphire substrate have a preferential orientation of the monoclinic (−713) plane (Joint Committee on Powder Diffraction Standards (JCPDS) no. 37-1468),[32] whereas those on the SiO_2/Si substrate are relatively randomly oriented and have low crystallinities.

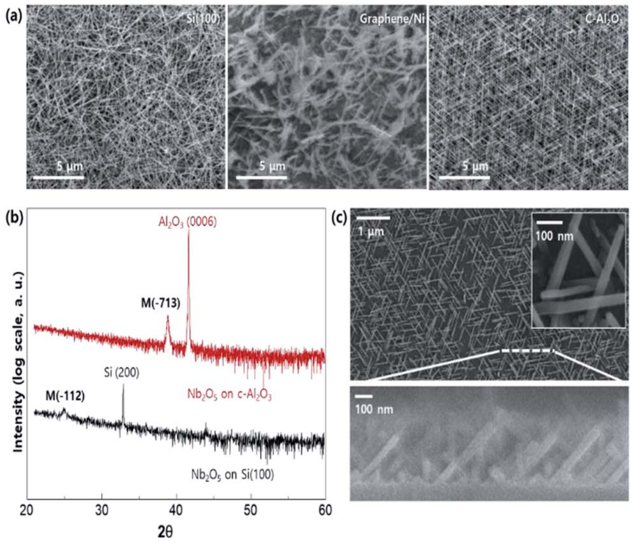

Fig. 1 (a) Scanning electron microscopy (SEM) images of Nb_2O_5 nanorods grown for 90 min on different substrates. (b) X-ray diffraction (XRD) patterns of Nb_2O_5 on c-plane sapphire (top) and Si (100) (bottom). (c) SEM images of Nb_2O_5 nanorods grown on c-plane sapphire for 30 min.

SEM images (Fig. 1c) of the sample obtained with a reduced deposition time (Fig. 1a and c show the samples deposited for 90 min and 30 min, respectively) confirm the preferential orientation of Nb_2O_5 deposited on the c-plane sapphire and reveal that equilateral triangular nanostructures were uniformly distributed with a tilting angle of approximately 45° with respect to the substrate.

TEM was performed to understand the regularity of the Nb_2O_5 nanorods grown on the c-plane sapphire crystal. As shown in Fig. 2a and b, the Nb_2O_5 nanorod with a (−112) growth direction has a tilting angle of 45.01° with respect to the (−713) plane, which is the preferred orientation, as shown in the XRD measurement (Fig. 2c and 1b). In addition, the result that no metallic component was detected in the head of the Nb_2O_5 nanorod reveals that Nb, decomposed from the $NbCl_5$ precursor, combines with remaining oxygen in the furnace to form Nb_2O_5 directly, referred to as vapour–solid growth mechanism.[33–35]

The X-ray pole figure of the Nb_2O_5/c-sapphire system was measured to understand the triangular arrangement of the nanorods. When the pole figure is measured at a tilting angle (χ) of 55°, the part with a 6-fold symmetry and that with a 3-fold symmetry are mixed, as shown in Fig. 3a and b. The sapphire (102) plane is tilted at 57.6° with respect to the (006) plane (referred to as c-plane) and has a 3-fold symmetry; therefore, the 3-fold symmetry (green circles in Fig. 3a) corresponds to the sapphire substrate. The remaining structures with the 6-fold symmetry can be attributed to the synthesised Nb_2O_5. Nb_2O_5, which has a monoclinic structure, usually has a 2-fold symmetry; however, it can have a 6-fold

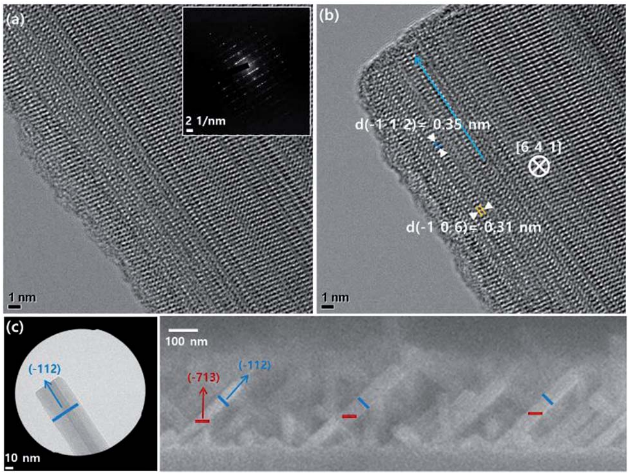

Fig. 2 (a and b) High-resolution TEM images and selected-area electron diffraction (SAED) pattern of a single Nb_2O_5 nanorod. The SAED pattern was recorded from the Nb_2O_5 nanorod shown in (c). (c) Low-magnification TEM image (left) and cross-section SEM image (right) of a single Nb_2O_5 nanorod.

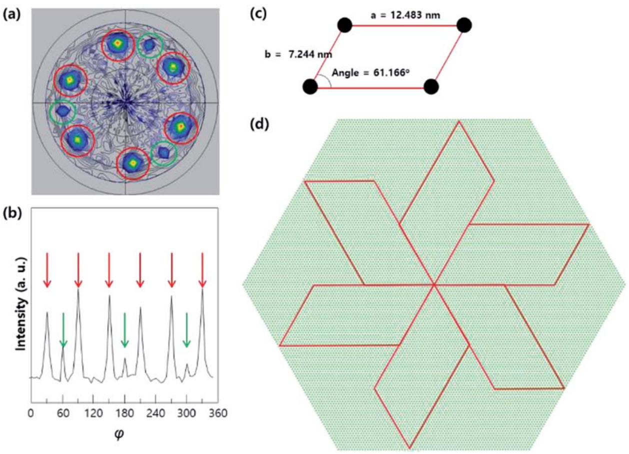

Fig. 3 (a) X-ray pole figure of the Nb_2O_5/c-sapphire system measured at a 2θ angle of 25.05° for the monoclinic Nb_2O_5 (−112) peak. Red and green circles represent the peaks of Nb_2O_5 nanorods and sapphire substrate, respectively. (b) Azimuthal (φ) scan data measured at a χ angle of 55°. (c) Cell shape of the monoclinic Nb_2O_5 (−713) plane. (d) Schematic of the hexagonal arrangement of the monoclinic Nb_2O_5 (−713) plane on the c-sapphire substrate.

symmetry if intervals of 120° are observed. Fig. 3c shows the cell shape of the monoclinic (−713) plane of Nb_2O_5 (a = 12.483 nm, b = 7.244 nm, α = 90°, and γ = 61.166°; the black circles represent O atoms). The epitaxial growth along the Nb_2O_5 (−713) plane on the c-plane sapphire substrate with an interatomic distance of 0.275 nm can be explained by domain matching epitaxy (DME).[36–38] The length of 45 atomic spacings of Al_2O_3 is 12.375 nm (0.275 nm × 45 = 12.375 nm), which implies a domain mismatch with the Nb_2O_5 a-axis of approximately 0.108 nm, while that of 3 atomic spacings of Al_2O_3 is 0.825 nm (0.275 nm × 3 = 0.825 nm), corresponding to a domain mismatch with the Nb_2O_5 b-axis of approximately 0.101 nm, leading to the hexagonal arrangement shown in Fig. 3d.

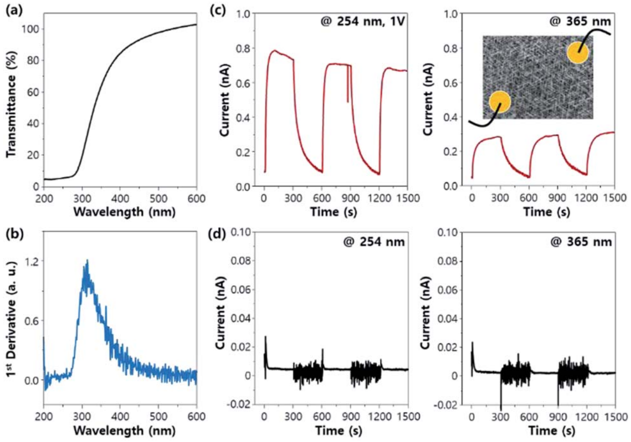

Fig. 4 (a) UV-visible transmittance spectrum of the Nb_2O_5/c-sapphire system and (b) its 1st derivative. Photo-conductivity of Nb_2O_5 grown on (c) c-sapphire and (d) Si (100) illuminated with lights with wavelengths of (left) 254 nm and (right) 365 nm at an applied voltage of 1 V.

The synthesised triangular radial Nb_2O_5 nanorods have excellent crystal qualities, which suggests that they have excellent properties in terms of UV absorption. Fig. 4a shows the UV-visible transmittance of the Nb_2O_5/c-sapphire sample. At approximately 400 nm, the light absorption is approximately 20%; with the decrease in the wavelength, the absorption increases (95% at 280 nm). As shown in the first-order differential form of the transmission spectrum (Fig. 4b), this absorption tendency is most prominent at approximately 300 nm, which implies that the synthesised Nb_2O_5 on c-sapphire can be effectively employed in a wide UV-detection range (from A to C). In addition, we could see the changes in the UV absorption behaviour through the comparison with the UV-visible transmittance spectrum of the sample grown for a longer time (Fig. S1†). As the synthesis time increased, the density of the nanorods increased and the nanorods were more cross-linked as shown in Fig. 1a and b, resulting in the change in the UV transmittance behaviour. Not only did the absolute amount of absorbed light increase, but also the absorption range was up-shifted by approximately 30 nm (see the change of the wavelength at which the slope of the graph changes from positive to negative). Furthermore, the relation of the UV-absorption to the synthesis temperature could also be deduced. As the synthesis temperature was lower, the density of nanorods decreased, and the nanorods were less cross-linked (see Fig. S2†). Based on the relationship between nanorods density and UV-absorption that we have seen above, it can be inferred that the higher the temperature, the greater the amount of UV absorbed.

The triangular radial Nb_2O_5 nanorods deposited on the c-sapphire substrate are connected to each other using a longer deposition time. Therefore, the system can be directly used as a UV-radiation detector without separation of nanorods and e-beam lithography process; *i.e.*, the device can be fabricated by directly depositing macroscale electrodes (shown in the inset schematics of Fig. 4c at a UV wavelength of 365 nm). In the Nb_2O_5/*c*-sapphire structure, distinct photoreactions are observed at UV wavelengths of 254 nm and 365 nm at an applied constant voltage of 1 V. The shorter UV wavelength provides a larger current (Fig. 4c). The current value increases as the applied voltage increases and has a linear relationship with the applied voltage. Fig. S3† shows the *I*–*V* curve of Nb_2O_5 grown on c-sapphire while illuminating UV light. The Nb_2O_5/Si structure exhibits photo-reactivity; however, the signal is very small, hindering its application as an actual device (Fig. 4d). Through this process, Nb_2O_5 nanorods with excellent crystallinities and self-connection can be easily employed for UV-radiation detection devices. The spectra responsivity (R_λ) and external quantum efficiency (EQE) are two critical parameters to show the performance of the UV detector.[12] They are expressed as $R_\lambda = \Delta I/PS$ and $\mathrm{EQE} = R_\lambda hc/e\lambda$, respectively, where ΔI is the difference between the photo-excited current and dark current, P is the light power density, S is the irradiated area, h is Planck's constant, c is the velocity of light, e is the electronic charge, and λ is the exciting wavelength. The calculated R_λ and EQE of the Nb_2O_5 on *c*-plane sapphire at 1 V are 1.87×10^{-3} A W^{-1} and 0.913% when irradiated with 254 nm UV and 1.76×10^{-4} A W^{-1} and 0.060% when irradiated by 365 nm UV. These values are difficult to compare with those of the other materials with nanowire (rod) network or mat structure as with ours reported in the literature because they were hardly evaluated by R_λ and EQE values, and even if evaluated, they were evaluated in microscale. These values are usually measured for a single nanowire,[39] nanobelt,[12] and nanoplate[13] between microscale electrodes in the literature. There was one paper that measured R_λ value of Nb_2O_5 nanomoss structure in macroscale, where the R_λ at 10 V is 2.43×10^{-3} A W^{-1} when irradiated with 365 nm UV.[14] Considering that a voltage 10 times higher than the voltage we applied was used, it can be inferred that the increased ΔI value due to the higher V led to the larger R_λ value than ours. The ΔI–V relationship for our sample is shown in Fig. S3.† However, the R_λ and EQE values of our sample are significantly smaller than those of single Nb_2O_5 nanobelt (15.2 A W^{-1} with 320 nm at 1 V)[12] and nanoplate (24.7 A W^{-1} with 320 nm at 1 V)[13] reported in other articles. Unlike them, our measurements are not on a single nanorod but on interconnected rods between the macroscale electrodes. Therefore, carrier transport must occur not only within nanorods but also between nanorods. In the case of transport between nanorods, carriers must overcome the junction barrier at the interface between the nanorods to move from one nanorod to another.[12,39,40] The low measured values can be attributed to the numerous transport processes that carriers experience when moving through the macroscale channel.

Conclusions

Nb_2O_5 nanostructures with excellent crystallinities were grown on *c*-plane sapphire and their UV-detection performance was measured. The grown Nb_2O_5 on the *c*-sapphire substrate had a 6-fold symmetry with DME on the substrate; the results confirmed the radial growth. Owing to the radial growth, the nanorods naturally connected when the deposition time increased. This structure can be used as a UV-radiation detector directly by depositing macroscale electrodes without separation of a single nanorod and e-beam lithography process. It was confirmed that electric reactions occur at different UV irradiation wavelengths (254 nm and 365 nm). Therefore, it is expected that the structure can be easily employed in the development of a large-area UV sensor.

Conflicts of interest

There are no conflicts to declare.

Acknowledgements

This research was supported by Basic Science Research Program through the National Research Foundation of Korea (NRF) funded by the Ministry of Education, Science and Technology (NRF-2018R1D1A1B07050253). We gratefully thank Tae-Woo Lee of RIAM (Research Institute of Advanced Materials) for XRD and Pole figure measurement.

Notes and references

1 X. Fang, Y. Bando, U. K. Gautam, T. Zhai, H. Zeng, X. Xu, M. Liao and D. Golberg, *Crit. Rev. Solid State Mater. Sci.*, 2009, **34**, 190–223.

2 K.-J. Chen, F.-Y. Hung, S.-J. Chang and S.-J. Young, *J. Alloys Compd.*, 2009, **479**, 674–677.

3 H. Wu, Y. Sun, D. Lin, R. Zhang, C. Zhang and W. Pan, *Adv. Mater.*, 2009, **21**, 227–231.

4 N. Gogurla, A. K. Sinha, S. Santra, S. Manna and S. K. Ray, *Sci. Rep.*, 2014, **4**, 6483.

5 Y. Xie, L. Wei, G. Wei, Q. Li, D. Wang, Y. Chen, S. Yan, G. Liu, L. Mei and J. Jiao, *Nanoscale Res. Lett.*, 2013, **8**, 188.

6 J. W. Schultze and M. Lohrengel, *Electrochim. Acta*, 2000, **45**, 2499–2513.

7 T. Proslier, J. Zasadzinski, L. Cooley, M. Pellin, J. Norem, J. Elam, C. Z. Antoine, R. A. Rimmer and P. Kneisel, *IEEE Trans. Appl. Supercond.*, 2009, **19**, 1404–1408.

8 S. Zhuiykov and E. Kats, *World Academy of Science, Engineering and Technology*, 2013, vol. 78, p. 484.

9 R. Jose, V. Thavasi and S. Ramakrishna, *J. Am. Ceram. Soc.*, 2009, **92**, 289–301.

10 H. Luo, W. Song, P. G. Hoertz, K. Hanson, R. Ghosh, S. Rangan, M. K. Brennaman, J. J. Concepcion, R. A. Binstead and R. A. Bartynski, *Chem. Mater.*, 2012, **25**, 122–131.

11 L. Alibabaei, H. Luo, R. L. House, P. G. Hoertz, R. Lopez and T. J. Meyer, *J. Mater. Chem. A*, 2013, **1**, 4133–4145.

12 X. Fang, L. Hu, K. Huo, B. Gao, L. Zhao, M. Liao, P. K. Chu, Y. Bando and D. Golberg, *Adv. Funct. Mater.*, 2011, **21**, 3907–3915.

13 H. Liu, N. Gao, M. Liao and X. Fang, *Sci. Rep.*, 2015, **5**, 7716.

14 R. Abdul Rani, A. S. Zoolfakar, N. S. Khairir, M. H. Mamat, S. Alrokayan, H. A. Khan and M. R. Mahmood, *J. Mater. Sci.: Mater. Electron.*, 2018, **29**, 1–10.

15 Z. Wang, Y. Hu, W. Wang, X. Zhang, B. Wang, H. Tian, Y. Wang, J. Guan and H. Gu, *Int. J. Hydrogen Energy*, 2012, **37**, 4526–4532.

16 R. A. Rani, A. S. Zoolfakar, J. Z. Ou, M. R. Field, M. Austin and K. Kalantar-Zadeh, *Sens. Actuators, B*, 2013, **176**, 149–156.

17 K. Sayama, H. Sugihara and H. Arakawa, *Chem. Mater.*, 1998, **10**, 3825–3832.

18 H. Kominami, K. Oki, M. Kohno, S.-i. Onoue, Y. Kera and B. Ohtani, *J. Mater. Chem.*, 2001, **11**, 604–609.

19 L. Sang, M. Liao and M. Sumiya, *Sensors*, 2013, **13**, 10482–10518.

20 H. Nakazawa, K. Sano, T. Abe, M. Baba and N. Kumagai, *J. Power Sources*, 2007, **174**, 838–842.

21 B. Reichman and A. J. Bard, *J. Electrochem. Soc.*, 1981, **128**, 344–346.

22 M. K. Siddiki, S. Venkatesan and Q. Qiao, *Phys. Chem. Chem. Phys.*, 2012, **14**, 4682–4686.

23 O. Wiranwetchayan, Z. Liang, Q. Zhang, G. Cao and P. Singjai, *Mater. Sci. Appl.*, 2011, **2**, 1697.

24 C. Soci, A. Zhang, B. Xiang, S. A. Dayeh, D. Aplin, J. Park, X. Bao, Y.-H. Lo and D. Wang, *Nano Lett.*, 2007, **7**, 1003–1009.

25 Y. Jiang, W. J. Zhang, J. S. Jie, X. M. Meng, X. Fan and S. T. Lee, *Adv. Funct. Mater.*, 2007, **17**, 1795–1800.

26 J.-J. Wang, F.-F. Cao, L. Jiang, Y.-G. Guo, W.-P. Hu and L.-J. Wan, *J. Am. Chem. Soc.*, 2009, **131**, 15602–15603.

27 L. Li, X. Fang, T. Zhai, M. Liao, U. K. Gautam, X. Wu, Y. Koide, Y. Bando and D. Golberg, *Adv. Mater.*, 2010, **22**, 4151–4156.

28 Y. Zhang, J. Wang, H. Zhu, H. Li, L. Jiang, C. Shu, W. Hu and C. Wang, *J. Mater. Chem.*, 2010, **20**, 9858–9860.

29 H. K. Yu and J.-L. Lee, *Sci. Rep.*, 2014, **4**, 6589.

30 D. T. Danielson, D. K. Sparacin, J. Michel and L. C. Kimerling, *J. Appl. Phys.*, 2006, **100**, 083507.

31 J. Guo, D. Ellis and D. Lam, *Phys. Rev. B*, 1992, **45**, 3204.

32 S. Heusing, D.-L. Sun, J. Otero-Anaya and M. A. Aegerter, *Thin Solid Films*, 2006, **502**, 240–245.

33 Y. Zhang, N. Wang, S. Gao, R. He, S. Miao, J. Liu, J. Zhu and X. Zhang, *Chem. Mater.*, 2002, **14**, 3564–3568.

34 A. Umar, S. Kim, Y.-S. Lee, K. Nahm and Y. Hahn, *J. Cryst. Growth*, 2005, **282**, 131–136.

35 Y. L. Chueh, M. W. Lai, J. Q. Liang, L. J. Chou and Z. L. Wang, *Adv. Funct. Mater.*, 2006, **16**, 2243–2251.

36 H. K. Yu and J.-L. Lee, *Cryst. Growth Des.*, 2010, **10**, 5200–5204.

37 F. Sánchez, R. Bachelet, P. de Coux, B. Warot-Fonrose, V. Skumryev, L. Tarnawska, P. Zaumseil, T. Schroeder and J. Fontcuberta, *Appl. Phys. Lett.*, 2011, **99**, 211910.

38 W.-R. Liu, Y.-H. Li, W. Hsieh, C.-H. Hsu, W. Lee, Y. Lee, M. Hong and J. Kwo, *Cryst. Growth Des.*, 2008, **9**, 239–242.

39 M. Chen, L. Hu, J. Xu, M. Liao, L. Wu and X. Fang, *Small*, 2011, **7**, 2449–2453.

40 S. Jeong, M. W. Kim, Y.-R. Jo, Y.-C. Leem, W.-K. Hong, B.-J. Kim and S.-J. Park, *Nano Energy*, 2016, **30**, 208–216.